Journal of ELECTRONIC MATERIALS, Vol. 46, No. 3, 2017
DOI: 10.1007/s11664-016-5206-x

The Impact of Surface Chemistry on Bio-derived Carbon Performance as Supercapacitor Electrodes

NIMAN H. ALSHAREEF,[1] DANIEL WHITEHAIR,[1] and CHUAN XIA [1,2]

1.—Materials Science and Engineering, King Abdullah University of Science and Technology (KAUST), Thuwal 23955-6900, Saudi Arabia. 2.—e-mail: chuan.xia@kaust.edu.sa

In this study, we demonstrate that highly functionalized and porous carbons can be derived from palm-leaf waste using the template-free facile synthesis process. The derived carbons have high content of nitrogen dopant, high surface area, and various defects. Moreover, these carbons exhibit a high electrical conductivity (107 S m^{-1}). Thanks to the high content of edge N (64.3%) and highly microporous nature (82% of microspores), these biomass-derived carbons show promising performance when used as supercapacitor electrodes. To be specific, these carbonaceous materials show a specific capacitance as high as 197 and 135 F g^{-1} at 2 and 20 A g^{-1} in three-electrode configuration, respectively. Furthermore, the symmetrical cells using palm-leaf-derived carbon show an energy density of 8.4 Wh Kg^{-1} at a power density of 0.64 kW Kg^{-1}, with high cycling life stability (~8% loss after 10,000 continuous charge–discharge cycles at 20 A g^{-1}). Interestingly, as the power density increases from 4.4 kW kg^{-1} to 36.8 kW kg^{-1}, the energy density drops slowly from 8.4 Wh kg^{-1} to 3.4 Wh kg^{-1}. Getting such extremely high power density without significant loss of energy density indicates that these palm-leaf-derived carbons have excellent electrode performance as supercapacitor electrodes.

Graphical Abstract

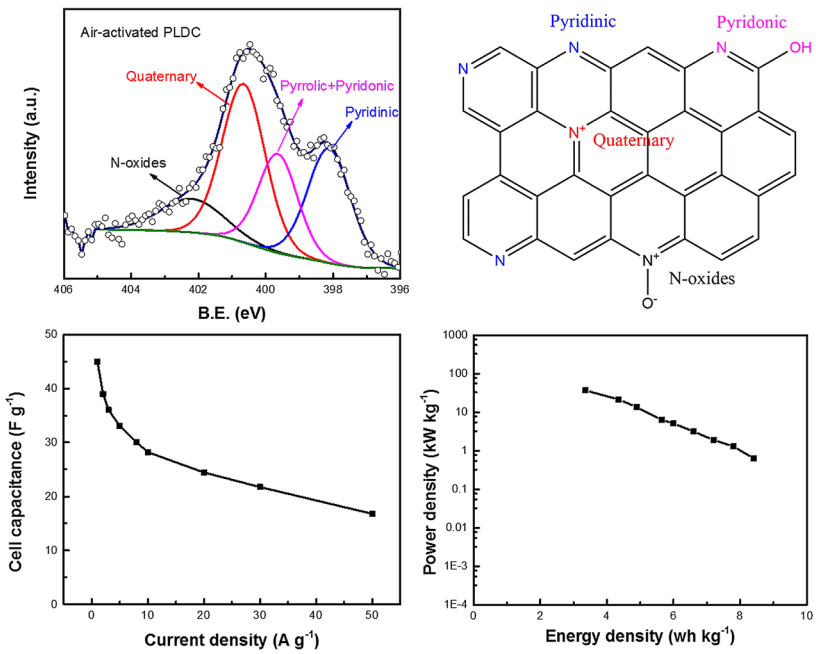

(Received August 5, 2016; accepted December 2, 2016; published online December 22, 2016)

Key words: Palm-leaf-derived carbon, supercapacitor, energy storage, high energy density

INTRODUCTION

Fabricating efficient electrical energy storage systems is of paramount importance for the advancement of electrical vehicles and renewable energy applications.[1,2] Nowadays, lithium ion batteries (LIBs) and supercapacitors (SCs) are recognized as the leading components in energy storage systems, where LIBs and SCs are, respectively, promising for high energy and high power density applications.[3–5] The increasing market size of hybrid vehicles has increased the demand for high-performance supercapacitors, where a high power device is needed to supply a surge during startup and to convert the kinetic energy associated with vehicle braking into useful electricity.[6] The SCs are categorized into electric double-layer capacitors (EDLCs) in which capacitance arises from charge accumulation in the electrode/electrolyte interface, and pseudocapacitors that are based on the fast and reversible redox reactions at the surface of electro-active materials.[7] Generally, the capacitance of pseudocapacitors is much higher than EDLCs. In most cases, these two mechanisms always work together. The current commercially available supercapacitors (in the form of EDLCs) are mainly based on carbonaceous electrode material, considering its low cost, high electrical conductivity, good chemical stability and impressive lifespan.[1,6,8–10] For example, in the commercial supercapacitor market, activated carbons (ACs) are regarded as the first candidate electrode materials and are already widely used in smart electronic devices. They are generally carbonized from wood, coal, etc.[11] However, the commercially available ACs offer limited control over specific surface area, conductivity and pore size distribution, always suffering from limited energy density (<5 Wh kg^{-1}).[1] While the surface area of ACs is the dominant factor to determine the performance of EDLCs, previous reports have also shown that, when the surface area of ACs reaches up to 3000 m^2 g^{-1}, they show a much lower specific capacitance (10 μF cm^{-2}) than their theoretical valve (15–25 μF cm^{-2}).[12,13] This is because most of the micropores with less than 0.4 nm diameter are inaccessible in the EDLCs. Therefore, there is a critical need to manufacture porous carbon with better supercapacitor performance (higher energy density compared to commercial ACs, simultaneously preserving their high power feature).

Over the years, efforts have been made to increase the performance of EDLCs, including preparation of carbons with designed pores[14,15] and the introduction of heteroatoms (N, O and B) into carbonaceous materials.[1,16] The latter approach has been demonstrated as a simple and powerful way towards high-energy EDLCs due to the pseudocapacitive contribution from the redox process of the heteroatom surface functionalities. Normally, the N-doped carbons can also deliver a higher electrical conductivity than their pristine counterparts. The incorporation of oxygen and nitrogen atoms into carbons have already been realized by oxidation of carbons and ammoniate treatment, respectively. However, these surface oxygen and nitrogen functional groups are not stable during cycling, leading to the fading of the pseudocapacitance.[12] Alternatively, pyrolysis of N-rich polymers has also been investigated for the preparation of N-doped carbons. However, the cost makes it practically undesirable. Utilizing sustainable biomass for energy storage application has received much attention in the scarcity of fossil energy. Thus, very recently, the daily biomass waste, which mainly contains protein, cellulose and lignin (e.g., eggshell, banana peel, silk), has been directly carbonized to produce heteroatom-doped carbons for SCs and LIBs applications.[1,6,8,11,12,17] The naturally high content of N and O in biomass always produces highly functionalized carbons after carbonization, which are very suitable for electrochemical energy storage application.

In this work, we investigate palm-leaf-derived carbon (PLDC) as electrode material for supercapacitor applications. We directly carbonized the palm leaves in argon atmosphere at 800°C, followed by air activation at 300°C. Our air-activated PLDCs contains 3.64% N and 12.83% O. This rich heteroatom doping can enhance the electrochemical reactivity and electronic conductivity, which improves electrode performance. In fact, the air-activated PLDCs show a specific capacitance of 196 F g^{-1} at 2 A g^{-1} and a cell capacitance of 45 F g^{-1} at 1 A g^{-1}, and an impressive cycling stability at very high current density ($\sim$92% capacitance retention after 10,000 cycles at 20 A g^{-1}).

EXPERIMENTAL

Materials Synthesis

The palm leaves used in the experiments were collected from palm trees in the campus of King Abdullah University of Science and Technology (KAUST). The collected biomaterial was extensively washed in ultrapure water and dried overnight in a vacuum oven. After cleaning with deionized (DI) water, the leaves were dried and carbonized at 800°C for 4 h in a tubular furnace with argon flow of

100 sccm, with a heating rate of 1°C min^{-1}. Then, the carbonized leaves were ground and washed. The obtained carbon powder was carefully washed in 20% KOH at 70°C for 6 h and 2.0 M HCl at 60°C for 12 h to remove the impurities. The purified samples were washed again using DI water. Finally, the as-prepared palm carbons were further activated at 300°C for 3 h under ambient air.

Structural Characterization

The morphology and microstructure of the samples were characterized by SEM (Nova Nano 630, FEI). XPS analysis was collected using Kratos AXIS Ultra DLD. The Raman spectroscopy was conducted on a Hariba LabRAM HR spectrometer. BET surface areas of the samples were determined using surface area and porosimetry system Micromeritics (ASAP 2420) at 77 K. Before measurements, the samples were dried at 70°C for 10 h in a vacuum oven and then degassed at 200°C for 6 h until the vacuum was less than 2 μm Hg. To evaluate the electrical conductivity, the carbon powders mixed with 10 wt.% binder were pressed into a thin film on the glass. Then, the conductivity of all samples was measured using a four-point electrical probe.

Electrochemical Measurements

The electrochemical tests were carried out at room temperature in both three-electrode (half-cell) and two-electrode (full-cell) configurations. In the three-electrode measurements, as-prepared carbons and polytetrafluoroethylene were mixed in a weight ratio of 90:10 for preparation of the working electrodes. A Pt wire was used as the counter electrode, and saturated Ag/AgCl as the reference electrode. Assembled coin cells for the two-electrode configuration were fabricated in which two identical pieces of the PLDC electrode samples ($\sim$3 mg of mass loading and $\sim$1 cm^2 of each electrode) were assembled, separated by a single layer separator (Celgard 3501), and placed inside a coin cell. All electrochemical measurements were carried out at room temperature using a VMP3 multichannel electrochemical workstation (Bio-Logic) by the techniques of electrochemical impedance spectroscopy, cyclic voltammetry (CV) and galvanostatic charge–discharge (CD). Carbon paper was used as current collector for as-prepared working electrode. We used 1.0 M H_2SO_4 as electrolyte for all measurements.

The absolute capacitance (C in F) was obtained from the galvanostatic CD curves according to the following equations.

$$C = \frac{I}{\frac{\Delta V}{\Delta t}}$$

where I is the constant current for CD and $\frac{\Delta V}{\Delta t}$ is slope of the discharge curve.[18] The specific capacitance and cell capacitance (C_{sp} and C_{cell} in F g^{-1}) were then calculated as:

$$C_{sp} = \frac{2C}{m}$$

$$C_{cell} = \frac{C}{2m}$$

where m is the mass loading of each electrode.

The key parameters of the supercapacitor, energy density (E) and power density (P), were calculated based on the total weight of the two electrodes in the full-cell devices according to the following equations.

$$E = \frac{1}{2} C_{cell} V^2$$

$$P = \frac{E}{\Delta t} = \frac{1}{2} C_{cell} V^2 / \Delta t$$

where C_{cell} is the cell capacitance calculated from CD curve, V is the voltage window applied during the CD measurement, and Δt is the discharge time obtained from the discharge curve.

RESULTS AND DISCUSSION

The microstructures of palm leaves, PLDC, and air-activated PLDC were investigated by scanning electron microscopy (SEM), as shown in Fig. 1a–c. It can be seen that the pristine palm leaves themselves show a highly porous structure. After carbonization and activation, the original porous frameworks were not destroyed, while the final products showed a rougher surface. These abundant macropores can facilitate the spread of the aqueous electrolyte on the entire surface of carbon materials, hence boosting the electrolyte ion trapping and access to the active sites.[19] Furthermore, SEM images revealed no obvious difference in PLDC strucutre before and after activation, because the pores introduced by the air activation process are mainly micropores. Raman spectroscopy analysis results of PLDC and air-activated PLDC are shown in Fig. 1d. The G band ($\sim$1600 cm^{-1}) is a characteristic feature of the graphitic layers and corresponds to the tangential vibration of the carbon atoms, while the D band ($\sim$1350 cm^{-1}) corresponds to the degree of disordered/defectiveness in the structure. The integral intensity ratio of these two peak (I_G/I_D) scales with the degree of the graphitic ordering in the carbons.[20] It is clear that our air-activated PLDCs show a more defective surface, with I_G/I_D = 0.93, compared to pure PLDCs. Thus, we believe that this air activation process can produce a more effective surface area, which is desirable for electrochemical energy storage applications. We further conducted N_2 adsorption–desorption measurements to determine the surface area and pore structures of our samples. As shown in Figure S1 and Table I, the calculated specific

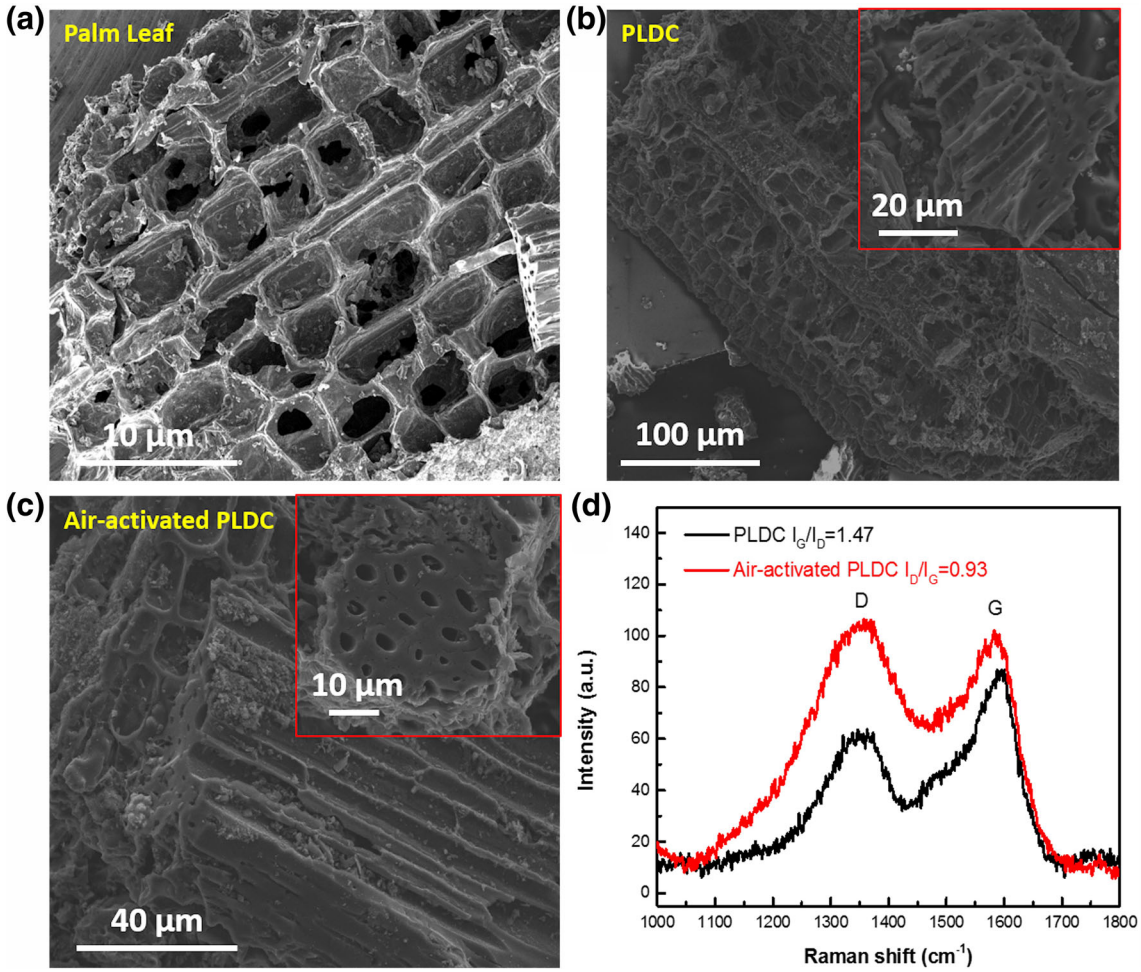

Fig. 1. SEM images of (a) palm leaf, (b) PLDC, and (c) air-activated PLDC. The insets of (b) and (c) are the high-resolution images of the selected sample. (d) The Raman spectra of PLDC and activated PLDC.

Table I. Physical and electrical properties of PLDC and air-activated PLDC

Sample	S_{BET} ($m^2\ g^{-1}$)[a]	S_{micro} ($m^2\ g^{-1}$)[b]	V_{total} ($cm^3\ g^{-1}$)[c]	Average pore size (nm)	Conductivity (S m^{-1})
PLDC	98.25	74.33	0.08	3.3	36
Air-activated PLDC	298.36	244.13	0.19	2.5	107

[a]BET surface area.[b]Surface area of micropores calculated by *t* plot method.[c]Total pore volume.

Brunauer–Emmett–Teller (BET) surface areas for PLDC and air-activated PLDC are 98.25 $m^2\ g^{-1}$ and 298.36 $m^2\ g^{-1}$ with the total pore volume of 0.08 $cm^3\ g^{-1}$ and 0.19 $cm^3\ g^{-1}$, respectively. The *t* plot method calculated micropores increased from 74.33 $m^2\ g^{-1}$ to 244.13 $m^2\ g^{-1}$ after air activation. The pore size distributions of PLDC before and after activation are similar, but the activated PLDC shows a higher concentration of micropores (82% compared with 76%). Obviously, the partial oxidation removal of carbon in hot air introduced higher surface area, porosity, and more suitable pore size (average pore size decrease from 3.3 nm to 2.5 nm) in our PLDC samples. What is more, the air-activated PLDC shows ~3 times higher electrical conductivity (107 S m^{-1}) than pure PLDC (36 S m^{-1}), even higher than activated carbon (43 S m^{-1}).[6] This enhancement has been ascribed to the doping effect of the electron-rich N in a graphitic layer. While the BET surface area of our air-activated PDLC is not as

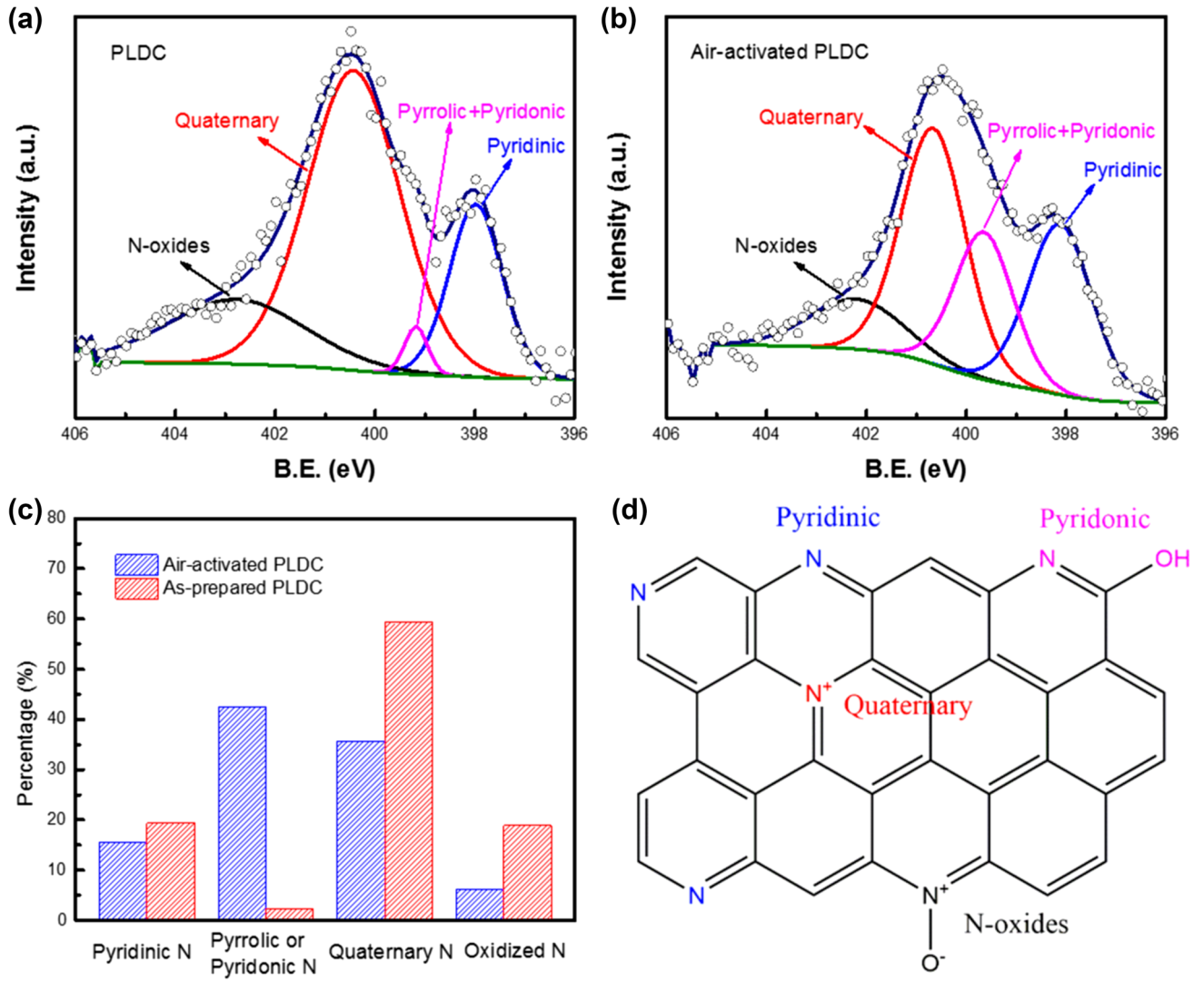

Fig. 2. Deconvoluted N 1 s spectra for PLDC before (a) and after (b) air activation. (c) Summary of the relative content of four different nitrogen species. (d) The corresponding atomic structure on the basis of XPS analysis.

comparable as commercial KOH-activated carbons (1000–3000 $m^2 g^{-1}$), we believe that this air activation process is more suitable for waste biomass (e.g., palm-leaf) carbonization based on the following considerations: (1) previous reports prove that the KOH-involved chemical activation process will destroy most of the N functional groups in the biomass[12]; (2) the original framework will be totally destroyed by KOH activation (Figure S2); (3) the corrosive KOH activation process always needs higher temperature (700–1000°C); and (4) the KOH activation process is more costly than activation in hot air.

X-ray photoelectron spectroscopy (XPS) was further employed to obtain the surface heteroatom content, which is very important for electrochemical performance. Figure S3 displays the survey spectra of PLDC and air-activated PLDC, showing the dominant elements to be C, N and O. The quantitative analyses demonstrate that the PLDC and air-activated PLDC contain a high content of N around 3.48 atm% and 3.64 atm%, respectively. This increase of N content indicates that the activation process introduces more N heteroatoms into PLDCs, and is superior to the KOH activation. The surface N functionalities are identified by the deconvolution of the high-resolution N 1 s core level peaks. Figure 2a and b elucidates the existence of four main nitrogen species,[21] that is, pyridinic (B.E. ~398.2 eV), pyrriolic or pyridonic (B.E. ~399.7 eV), quaternary (B.E. ~400.7 eV) and nitrogen oxides (B.E. ~402.3 eV) in PDLC and air-activated PDLC samples. Figure 2d clearly displays the corresponding atomic structures of above-mentioned four nitrogen species. The percentage of each component of these four nitrogen species are summarized in

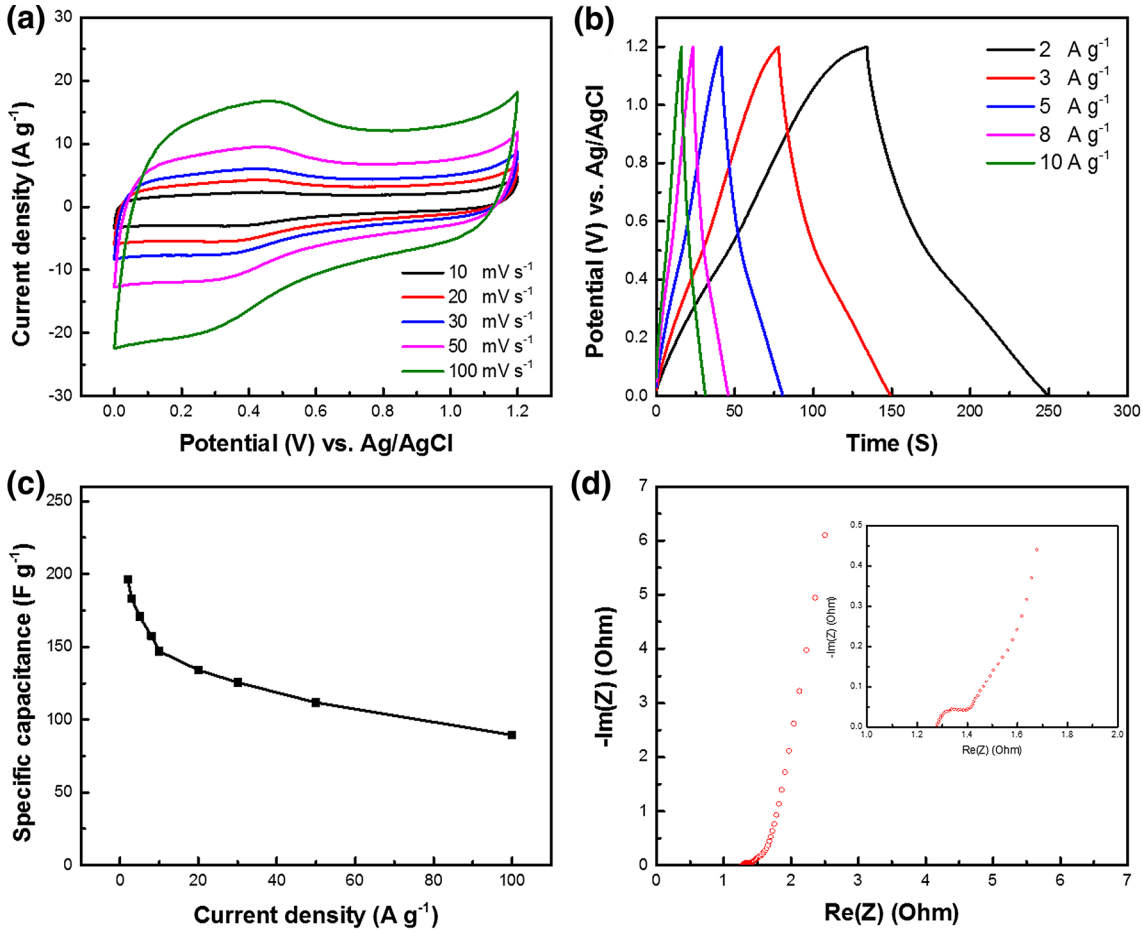

Fig. 3. Electrochemical performance of air-activated PLDCs in a three-electrode setup. (a) Cyclic voltammograms and (b) galvanostatic charge–discharge curves in 1.0 M H_2SO_4 at different conditions. (c) Gravimetric capacitances obtained from various charge–discharge current densities. (d) Nyquist plots in 1.0 M H_2SO_4.

Fig. 2c. Interestingly, we observed an apparent increase of the pyrriolic or pyridonic N with an obvious decrease of quaternary N after air activation. This indicates the middle-located N is partially converted to edge N functional groups. It is known that edge-site N is more active than middle-located N (e.g., quaternary N) in electrochemical applications. Hence, the air activation process makes our PLDCs more electrochemically active. It is also worth noting that our air-activated PLDC presents a very high content of edge N (64.3%), whereas that of PLDC is 40.7%. Moreover, we also deconvoluted the O 1*s* core level peaks of air-activated PLDC, as shown in Figure S4. This shows that there are three types of oxygen functionalities on the surface of air-activated PLDC: C=O groups (B.E. ~531.5 eV), C–OH and/or C–O–C groups (B.E. ~533.2 eV), and carboxylic groups (B.E. ~535.8 eV).[6] These functional groups make the samples more hydrophilic which is beneficial for electrochemical performance in aqueous electrolytes. Otherwise, these O functionalities also serve as active sites for fast surface redox reactions, contributing to the higher specific capacitance in EDLCs. Thus, from the BET and XPS analysis, we can concluded that highly functionalized porous carbons have been prepared from palm leaves.

The electrochemical performance of supercapacitors using PLDC electrodes in the three-electrode configuration is shown in Fig. 3. We used 1.0 M H_2SO_4 aqueous solution as electrolyte. Figure 3a shows the results of cyclic voltammetry (CV) measurements of air-activated PLDC under different scan rates. The quasi-rectangular CV curves demonstrate a typical EDLC-like behavior of these electrodes. However, the obvious Faradaic humps at different scan rates are observed, which suggest that the capacitive response is due to the synergistic effect of electrical double-layer formation and redox reactions.[1] The prominent redox peaks shown in the CV curves can be attributed to the fast Faradaic reactions of the surface N and O functionalities. At the scan rate of 100 mV s^{-1}, the PLDC electrodes still retain a quasi-rectangular shape, indicating a fast and efficient mass and charge transfer rate. This can be ascribed to the proper pore distribution and high

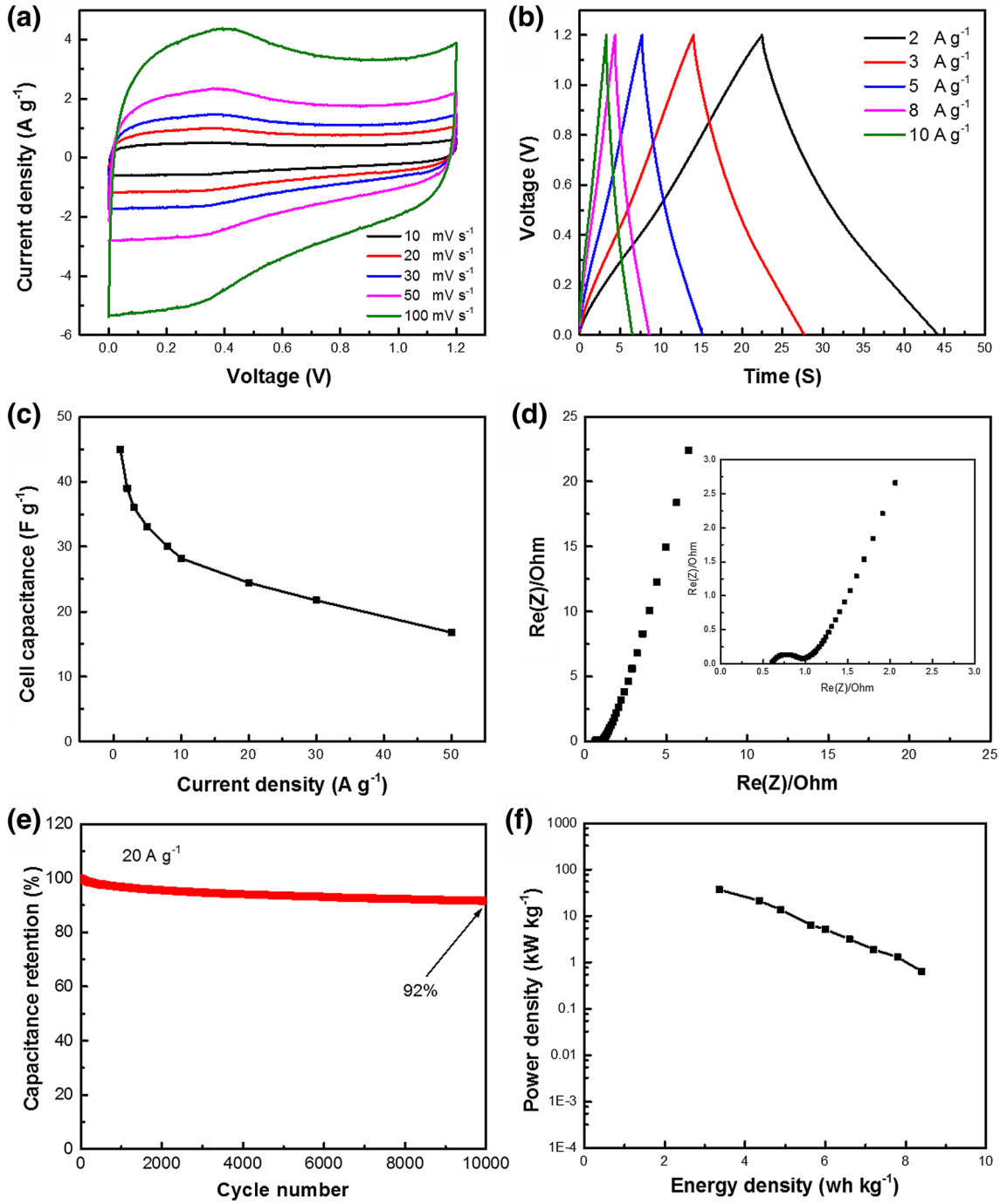

Fig. 4. Electrochemical performance of symmetrical supercapacitors using air-activated PLDCs as working electrodes. (a) CV and (b) CD curves; (c) gravimetric cell capacitances obtained from various charge/discharge current densities; (d) Nyquist plots in 1.0 M H_2SO_4. (e) Long-term cycling stability measurement at current density of 20 A g^{-1}. (f) Ragone plots of the symmetric cells.

surface area of our electrodes. The galvanostatic CD (CD) curves (Fig. 3b) show symmetric mirror-like features of the charge and discharge process at different current densities, implying the high efficiency of the supercapacitive performance and highly reversible redox reactions taking place in the air-activated PLDC electrodes. All the CD curves show a negligible voltage drop (IR), which indicates the low value of equivalent series resistance (ESR). These excellent electrochemical features are believed to contribute to high power output from the supercapacitors.[22] Figure 3c summarizes the CD-derived specific capacitance (C_{sp}) of air-activated PLDC electrodes. At the current density of 2 A g^{-1}, a high C_{sp} of 197 F g^{-1} was obtained. This value is much higher than that of commercial ACs (~100 F g^{-1}).[11,23,24] In

addition, the C_{sp} obtained in this work are higher than carbon obtained from other materials, including silk protein (168 F g^{-1} at 0.8 A g^{-1}),[25] leaves (88 F g^{-1} at 2 A g^{-1}),[26] fungi (170 F g^{-1} at 10 mV s^{-1})[11] wood (180 F g^{-1} at 10 mV s^{-1}),[27] carbide-derived carbon (129 F g^{-1} at 10 mV s^{-1}),[28] activated silicon carbide-derived carbon (138 F g^{-1} at 0.1 A g^{-1}),[29] novolac-derived carbon (127 F g^{-1} at 1 A g^{-1}),[30] etc. Notably, at the high current density of 20 A g^{-1}, the specific capacitance of the air-activated PLDC sample can still be up to 135 F g^{-1}, corresponding to a high rate capability of 69%. Even at the very high scan rate of 100 F g^{-1}, this electrode still retained 47% of its initial specific capacitance, demonstrating good rate performance. Figure 3d presents the Nyquist plot of the air-activated PLDC electrode. It is clear that this electrode shows a typical supercapacitve performance with the ESR and charge transfer (R_{ct}) resistances of ~1.28 Ω and ~0.18 Ω, respectively. Such a low resistivity is believed to be due to bulk N, which is known to increase the electrical conductivity of carbons.[31] Undoubtedly, such a high electrical conductivity is very desirable for high-power supercapacitors. It is worth noting that the supercapacitor performance of our pristine PLDCs are much worse than the activated samples, as shown in Figure S5. The air-activated PLDC shows ~5.6-times higher specific capacitance than the pure PLDC sample, as well as better rate performance. Moreover, the activated PLDCs can deliver higher electrical conductivity (from the Nyquist plot in Figure S5d), in agreement with our direct four-point probe measurements. This comparison clearly demonstrates that such a simple air activation process is effective to enhance the supercapacitve performance of biomass-derived carbons.

We further evaluated the air-activated PLDCs using a symmetric two-electrode configuration. Figure 4a and b shows the CV and CD curves of air-activated PLDC cells. It obvious that the cells exhibit an ideal supercapacitor performance (quasi-rectangular CVs and symmetrical CDs at all test conditions). Further, as shown in Fig. 4c, the cell capacitance was calculated as 45 F g^{-1} and 18 F g^{-1} at current densities of 1 A g^{-1} and 50 A g^{-1}, respectively. Even though current density increased by a factor of 50, 40% of its initial capacitance can be retained. The Nyquist plot of the as-made symmetrical cell is shown in Fig. 4d. It can be seen that the devices have excellent electrical conductivity with a very small cell resistance (~0.6 Ω) at a high frequency. The R_{ct} is merely ~0.3 Ω, implying the high-power feature of these cells. As a critical parameter to determine the energy storage performance for practical applications, the long-term cycling stability of our symmetric cell was tested at the very high current density of 20 A g^{-1} and is shown in Fig. 4e. After 10,000 electrochemical cycles, the air-activated PLDC cell retains ~92% of its initial capacitance which demonstrates that these activated PLDC are very stable for supercapacitor applications. The energy and power density of the devices with activated PLDC are shown in the Ragone plot in Fig. 4f. The optimized symmetrical supercapacitors using activated PLDC show an energy of 8.4 Wh Kg^{-1} at a power density of 0.64 kW Kg^{-1}. What is more, it is worth noting that, with the increase of power density from 4.4 kW kg^{-1} to 36.8 kW kg^{-1}, the energy densities drop slowly from 8.4 Wh kg^{-1} to 3.4 Wh kg^{-1}. Getting an extremely high power density without much drop in energy density indicates that the activated PLDC possess significantly enhanced electrochemical performance as supercapacitor electrodes.[22] Furthermore, the energy and power densities we achieved here are superior to commercial AC-based supercapacitors.

CONCLUSION

In summary, we have demonstrated that high-performance supercapacitors can be fabricated using palm-leaf-derived carbon, termed PLDC, as electrodes. We show that these highly functionalized and porous carbons can be prepared using the template-free facile synthesis process. The air-activated PLDCs exhibit high surface area, defects, and a relatively high N-doping level. Moreover, 64.3% of the surface nitrogen heteroatoms are located at edge sites, which is highly desirable for supercapacitor applications. The activated PLDCs deliver a specific capacitance and cell capacitance as high as 197 F g^{-1} and 45 F g^{-1}, respectively. The values we obtained are much better than commercial ACs and previousky reported biomass-derived carbons. Furthermore, the symmetrical PLDC cells show an energy density of 8.4 Wh Kg^{-1} at a power density of 0.64 kW Kg^{-1}, with high cycling life stability (~8% loss after 10,000 continuous CD cycles at 20 A g^{-1}). Our results indicate that these renewable PLDC electrodes are potential alternatives for commercial AC-based supercapacitors, considering their very low cost and abundance.

ACKNOWLEDGEMENTS

Research reported in this publication has been supported by King Abdullah University of Science and Technology (KAUST). NHA would like to thank the KAUST High School staff, particularly Dr. Christos N. Hadjichristidis for several useful discussions, and Ms. Edwige Thivin-Boutry for her kind advice throughout the personal project research.

ELECTRONIC SUPPLEMENTARY MATERIAL

The online version of this article (doi: 10.1007/s11664-016-5206-x) contains supplementary material, which is available to authorized users.

REFERENCES

1. J.H. Hou, C.B. Cao, F. Idrees, and X.L. Ma, *ACS Nano* 9, 2556 (2015).
2. J. Yan, Q. Wang, T. Wei, and Z.J. Fan, *Adv. Energy Mater.* 4, 1300816 (2014).
3. S.M. Chen, R. Ramachandran, V. Mani, and R. Saraswathi, *Int. J. Electrochem. Sci.* 9, 4072 (2014).
4. V. Etacheri, R. Marom, R. Elazari, G. Salitra, and D. Aurbach, *Energy Environ. Sci.* 4, 3243 (2011).
5. B. Ahmed, C. Xia, and H.N. Alshareef, *Nano Today.* 11, 250 (2016).
6. Z. Li, Z.W. Xu, H.L. Wang, J. Ding, B. Zahiri, C.M.B. Holt, X.H. Tan, and D. Mitlin, *Energy Environ. Sci.* 7, 1708 (2014).
7. C. Xia, W. Chen, X.B. Wang, M.N. Hedhili, N.N. Wei, and H.N. Alshareef, *Adv. Energy Mater.* 5, 1401805 (2015).
8. E.M. Lotfabad, J. Ding, K. Cui, A. Kohandehghan, W.P. Kalisvaart, M. Hazelton, and D. Mitlin, *ACS Nano* 8, 7115 (2014).
9. L.L. Zhang and X.S. Zhao, *Chem. Soc. Rev.* 38, 2520 (2009).
10. H. Zanin, E. Saito, H. Ceragioli, V. Baranauskas, and E. Corat, *Mater. Res. Bull.* 49, 487 (2014).
11. H. Zhu, X.L. Wang, F. Yang, and X.R. Yang, *Adv. Mater.* 23, 2745 (2011).
12. Z. Li, L. Zhang, B.S. Amirkhiz, X. Tan, Z. Xu, H. Wang, B.C. Olsen, C. Holt, and D. Mitlin, *Adv. Energy Mater.* 2, 431 (2012).
13. B.E. Conway, *Electrochemical Supercapacitors: Scientific Fundamentals and Technological Applications*, 1st ed. (New York: Kluwer Academic/Plenum, 1999).
14. C.O. Ania, V. Khomenko, E. Raymundo-Piñero, J.B. Parra, and F. Béguin, *Adv. Funct. Mater.* 17, 1828 (2007).
15. A. Stein, Z. Wang, and M.A. Fierke, *Adv. Mater.* 21, 265 (2009).
16. Z. Wen, X. Wang, S. Mao, Z. Bo, H. Kim, S. Cui, G. Lu, X. Feng, and J. Chen, *Adv. Mater.* 24, 5610 (2012).
17. Z. Li, Z. Xu, X. Tan, H. Wang, C.M. Holt, T. Stephenson, B.C. Olsen, and D. Mitlin, *Energy Environ. Sci.* 6, 871 (2013).
18. V. Khomenko, E. Frackowiak, and F. Beguin, *Electrochim Acta.* 50, 2499 (2005).
19. C. Xia, Q. Jiang, C. Zhao, M.N. Hedhili, and H.N. Alshareef, *Adv. Mater.* 28, 77 (2016).
20. J. Ding, H.L. Wang, Z. Li, A. Kohandehghan, K. Cui, Z.W. Xu, B. Zahiri, X.H. Tan, E.M. Lotfabad, B.C. Olsen, and D. Mitlin, *ACS Nano* 7, 11004 (2013).
21. B. Kumar, M. Asadi, D. Pisasale, S. Sinha-Ray, B.A. Rosen, R. Haasch, J. Abiade, A.L. Yarin, and A. Salehi-Khojin, *Nat. Commun.* 4, 2819 (2013).
22. C. Xia, W. Chen, X. Wang, M.N. Hedhili, N. Wei, and H.N. Alshareef, *Adv. Energy Mater.* 5, 1401805 (2015).
23. P. Simon and Y. Gogotsi, *Nat. Mater.* 7, 845 (2008).
24. C.M. Parlett, K. Wilson, and A.F. Lee, *Chem. Soc. Rev.* 42, 3876 (2013).
25. Y.S. Yun, S.Y. Cho, J. Shim, B.H. Kim, S.J. Chang, S.J. Baek, Y.S. Huh, Y. Tak, Y.W. Park, and S. Park, *Adv. Mater.* 25, 1993 (2013).
26. M. Biswal, A. Banerjee, M. Deo, and S. Ogale, *Energy Environ. Sci.* 6, 1249 (2013).
27. F.-C. Wu, R.-L. Tseng, C.-C. Hu, and C.-C. Wang, *J. Power Sources* 144, 302 (2005).
28. B. Dyatkin, O. Gogotsi, B. Malinovskiy, Y. Zozulya, P. Simon, and Y. Gogotsi, *J. Power Sources* 306, 32 (2016).
29. E. Tee, I. Tallo, T. Thomberg, A. Jänes, and E. Lust, *J. Electrochem. Soc.* 163, A1317 (2016).
30. B. Krüner, J. Lee, N. Jäckel, A. Tolosa, and V. Presser, *ACS. Appl. Mater. Inter.* 8, 9104 (2016).
31. P. Serp and J.L. Figueiredo, *Carbon Materials for Catalysis* (NJ: Wiley, 2009), p. 219.